Please cite this article as: J.Li and A.S.Morgans, Simplified models for the thermodynamic properties along a combustor and their effect on thermoacoustic instability prediction, Fuel, 184 (2016) 735-748.
http://dx.doi.org/10.1016/j.fuel.2016.07.050

Simplified models for the thermodynamic properties along a combustor and their effect on thermoacoustic instability prediction

Jingxuan Li, Aimee S. Morgans*

Department of Mechanical Engineering, Imperial College London, London, UK

Abstract

Accurately predicting the thermoacoustic modes of a combustor depends upon knowledge of the thermodynamic properties within the combustor; flame temperature, heat release rate, speed of sound and ratio of specific heats all have a strong effect. Calculating the global equilibrium properties resulting from fuel combustion is not straightforward due to the presence of complex multi-species and multi-step reaction mechanisms. A method which decouples the calculations of species dissociations is proposed in this work: this improves the precision of calculation when using few species and reduces the computational cost and complexity to a degree that embedding within low order thermoacoustic network codes is feasible. When used to calculate the combustion product mole fractions, temperature, heat release rate, speed of sound and ratio of specific heats for hydrocarbon-air flames, the method is found to be accurate and highly efficient across different operating conditions and fuel types. The method is then combined with improved low-order wave-based network modelling, the latter employing wave-based acoustic models which account for the variation of thermodynamic properties along the combustion chamber. For a laboratory-scale combustor with a large downstream temperature variation, it is shown that accurate prediction of thermoacoustic modal frequencies and growth rates does depend on accounting for the variation in thermodynamic properties.

Keywords: Combustion instabilities, Thermodynamic equilibrium properties, Thermoacoustic instability prediction, Low-order wave-based network modelling, Temperature distribution

1. Introduction

For both modern industrial gas turbines and aero-engines, lean premixed combustion offers the prospects of reducing NO_x emission while keeping other pollutants, e.g., CO, at low levels [1]. Unfortunately, lean premixed systems are highly susceptible to combustion instabilities, also known as thermoacoustic instabilities, which may lead to an early ageing of the combustion chamber or in extreme cases to severe structural damage [2, 3]. The thermoacoustic stability of a combustor is determined by the balance between the energy gain from the heat released from unsteady combustion and the dissipation due to the viscous thermal damping [3, 4], radiation from the boundaries [5] and various relaxation processes in flows with particles or droplets [2]. Flame perturbations arise in different ways and originate mainly from the convection of hydrodynamic perturbations [2] or disturbances in the fuel and air injection supplies [6, 7]. These are susceptible to acoustic disturbances, and may lead to flame wrinkles that are convected along the flame front, modifying the flame surface area due to spatially non-uniform hydrodynamic perturbations [8–11] and inhomogeneous reactant mixture compositions [3] .

*Corresponding author.
Email addresses: ljx.buaa@gmail.com (Jingxuan Li), a.morgans@imperial.ac.uk (Aimee S. Morgans)

Accepted by Fuel Journal *August 12, 2016*

Prediction and suppression of combustion instabilities at the early design stage of a gas turbine thus are a priorty, but this still constitutes a challenge due to the complex mechanisms and combustor geometries involved [2, 12]. Approaches for analysing combustion instabilities generally fall within two categories. The first involves direct numerical calculation of the coupled acoustic oscillations and unsteady heat release from flames within the combustor, via complete 3D compressible Computational Fluid Dynamics (CFD) simulations [13]. Recent work investigated self-excited azimuthal modes using parallel LES in a full scale helicopter combustion chamber [14]. These simulations are highly costly and difficult to extend to industry analysis.

An alternative approach is to decouple calculation of the acoustic waves and the unsteady flame response. The response of the unsteady heat release rate from the flame to acoustic disturbances can be characterised via a flame transfer function (FTF) for linear analysis [15], or a flame describing function (FDF) for (weakly) nonlinear analysis [16]. These can be obtained from experiments [17, 18], analytical models [15, 16, 19, 20] or numerical simulations [21, 22]. The generation, propagation and reflection/transmission of acoustic waves can be captured by either a low order acoustic network model or a Helmholtz solver, both of which exploit the fact that the acoustic wave behaviour is linear for lean premixed gas-turbine combustors [23]. The former simplifies the combustor geometry to series of simple modules, assumes that the acoustic wave behaviour is low-dimensional, typically just longitudinal and circumferential waves, and hence relates acoustic wave strength between modules using the flow conservation equations. The latter assumes zero time-averaged flow velocity and describes the acoustics using the Helmholtz equation [24, 25]. The acoustics and flame models are then combined in order to predict the thermoacoustic modes of the combustor.

It should also be noted that intrinsic flame instability owing to strong coupling mechanisms between combustion and flow perturbations occurs when the flame front propagates into premixed reactants confined by a duct [9, 26, 27]. This type of instability differs from the system instability presented above and is out of scope of the present study.

Accurately predicting these thermoacoustic modes requires the time-averaged thermodynamic properties within the combustor, such as flow temperature, speed of sound and ratio of specific heats, to be known. In practice, these will vary spatially, particularly across the flame due to the large temperature change, but also downstream of it if temperature gradients are present. Despite this, most low-order thermoacoustic analyses assume that these properties are uniform within the combustor. Many analytically implemented methods assume that some thermodynamic properties such as ratio of specific heats and heat capacities are constant over the whole combustor, including across the flame, despite the large temperature increase. Computationally-implemented methods tend to account for the difference across the flame only, predicting downstream properties using simple temperature dependent empirical formulae for air or a single species [28–30]. These approximations break down for richer flames and high temperature configurations due to dissociations of species. Furthermore, for long combustion chambers, smooth temperature changes along the combustor may lead to spatial variation in other thermodynamic properties, which should not be neglected [31]. Although the thermodynamic properties can be calculated using separate chemical simulations, this greatly increases the computational time and complexity of low-order network modelling, requiring recourse to an external calculation tool for every change in flow or flame conditions.

In this work, highly simplified and therefore computationally fast methods for calculating the global equilibrium properties of the combustion products are suggested. This provides a means of rapidly calculating the time-averaged thermodynamic properties either side of the flame; the methods are simple enough for embedding within low order thermoacoustic tools, allowing the effect of properties such as temperature, heat release rate, speed of sound and ratio of specific heats of combustion products to be efficiently accounted for.

Calculating the global equilibrium properties of fuel combustion is not straightforward due to the complex multi-species and multi-step reaction mechanisms at play, especially when mixture compositions oscillate with time at considerable frequencies. Even in CFD simulations, reduced step schemes are widely used to model the complex combustion process [12, 13, 32, 33]. Calculations which account for relatively few species (e.g., 6 major species CO_2, CO, H_2O, H_2, O_2 and N_2 for hydrocarbon-air combustion) are still not straightforward since multiple partial equilibrium equations with multiple unknowns need to be simultaneously determined, which becomes even more complicated when the flame temperature is also yet to be determined.

This work proposes a simplified method which decouples the calculations of species dissociations, in order to reduce the calculation cost and improve the calculation precision when using few species. This method is applied to the combustion products of hydrocarbon-air flames: the calculation of mole fractions (Section 2), flame temperature (Section 3) and speed of sound and ratio of specific heats (Section 4) is performed. Validation is carried out by changing the equivalence ratio, initial temperature, ambient pressure and fuel, and comparing results to those computed using

the CANTERA code [34] with the GRI-Mech 3.0 mechanism, comprising 325 elementary chemical reactions with associated rate coefficient expressions and thermochemical parameters for the 53 species. In Section 5, these methods are successfully applied to a well-documented laboratory-scale combustor comprising a long combustion chamber. The time-averaged temperature changes from 1591 K at the flame position to 1193 K at the downstream end, and so the effect of spatial changes in thermodynamic properties on the thermoacoustic modes cannot be neglected. An improved low order wave-based network modelling is proposed, which accounts for these changes. It is shown that by accounting for the spatial profiles in the thermodynamic properties, prediction of the thermoacoustic modes is improved. Conclusions are drawn in the final section.

2. Calculation of the global equilibrium combustion product composition

Fuel combustion is a complex process, comprising multiple species undergoing multiple chemical reactions. The reaction time for each chemical reaction differs, and the species and corresponding mole fractions in the combustion products change with time. Assuming that the reaction time for each elementary reaction is sufficiently small, a global chemical equilibrium may be attained rapidly [35]. The combustion products can then be considered "frozen" since the global reaction time is sufficiently small compared to the convection time of the flow disturbances, e.g., perturbations in the fresh reactant mixture composition. The composition of the global equilibrium at a required instant can thus be resolved using the corresponding fresh mixture properties at that instant. For each elementary reaction, partial chemical equilibrium is attained when the chemical potential, e.g. Gibbs free energy, is minimised, and can be mathematically described using an equilibrium constant [36, 37]. For example, for the elementary reaction $CO_2 \rightleftharpoons CO + 0.5O_2$, the equilibrium constant can be expressed as:

$$K_{p,1} = \frac{\left(p_{CO}/p_0\right)^{n_{CO}}\left(p_{O_2}/p_0\right)^{n_{O_2}}}{\left(p_{CO_2}/p_0\right)^{n_{CO_2}}} = \exp\left(-\Delta G^0_{T,1}/RT\right) \tag{1}$$

where, $\Delta G^0_{T,1}$ is the standard-state Gibbs free energy change of this elementary reaction, $R = 8.3145$ J mol^{-1} K^{-1} is the gas constant, $p_{\mathcal{M}_k}$ denotes the partial pressure of species $\mathcal{M}_k$ and $p_0 = 101325$ Pa is the standard-state pressure. $n_{CO_2} = 1$, $n_{CO} = 1$ and $n_{O_2} = 0.5$ are mole numbers of corresponding species in the elementary reaction. The equilibrium constant K_p changes with temperature, e.g., the evolution of $K_{p,1}$ with temperature T is shown in Fig. 1. With increasing temperature, the equilibrium shifts to products, changing the mixture composition in the final products. To determine the equilibrium composition of the combustion products, a large number of partial equilibrium equations, e.g. $CO_2 \rightleftharpoons CO + 0.5O_2$, are needed to close the system. It was suggested in [35, 38] that the minimum number of elementary reactions n_e satisfies $n_e = n_s - n_k$, where n_s is the number of chemical species present in the final products and n_k is the number of indivisible elements or atoms within the reactive mixture. Calculation of the equilibrium composition is thus not straightforward and solution of such multi-species and multi-step reaction mechanisms are still relatively costly, especially when disturbances in mixture composition oscillate with time at considerable frequencies. Even in CFD simulations, reduced step schemes are still widely used to model the combustion process [32, 33].

A reduced order scheme is proposed in this work to simplify the calculation of mixture composition for thermoacoustic stability analysis. As presented above, the calculation cost increases with the number of species accounted for in the products. To simplify the calculation, we only account for the major species, with the combustion products assumed to be CO_2, CO, H_2O, H_2, O_2 and N_2 for hydrocarbon-air combustion, although minor species are also present due to dissociations of major species at high temperature ($T > 1200$ K), even for lean premixed flames [36]. Nevertheless, the combustion reaction for an arbitrary hydrocarbon-air flame can be simplified as:

$$C_xH_y + a(O_2 + 3.76N_2) \rightarrow \nu_1CO_2 + \nu_2CO + \nu_3H_2O + \nu_4H_2 + \nu_5O_2 + 3.76aN_2 \tag{2}$$

where $a = (x + y/4)/\phi$ denotes the ratio of the mole number of O_2 in the fresh reactants to that of fuel, and can be considered as a known constant, once the fuel type and mixing equivalence ratio ϕ are given. Air is assumed to consist of only O_2 and N_2 [37], as represented in the second component on the left side of Eq. (2). ν_k, $1 \le k \le 5$ are the coefficients of the five major species in the combustion products. One now has four indivisible elements, C-, H-, O- and N-atoms. The minimum required elementary equilibrium reaction depends on the number of species present in the combustion products, which changes with equivalence ratio ϕ, initial ambient pressure p_0, initial temperature T_0 [37], combustion efficiency [39], dilution rate [33], etc.

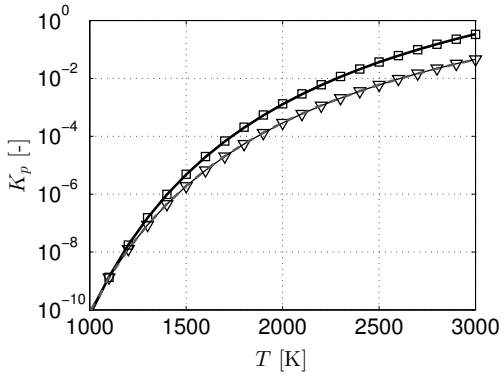

Figure 1: Evolution of equilibrium constants K_p with temperature T. Markers □ and ▽ represent the equilibrium constants $K_{p,1}$ and $K_{p,2}$ of partial equilibrium equations $CO_2 \rightleftharpoons CO + 0.5O_2$ and $H_2O \rightleftharpoons H_2 + 0.5O_2$, respectively. These data are obtained using the seventh degree NASA polynomial, which are available on the NASA Glenn Research Center website (`http://www.grc.nasa.gov/WWW/CEAWeb/ceaHome.htm`). The two continuous lines represent their low degree fittings: $\check{K}_{p,1} = \exp\left((84T - 2.79 \times 10^5)/RT\right)$ and $\check{K}_{p,2} = \exp\left((57.8T - 2.51 \times 10^5)/RT\right)$, which are used in later calculations.

2.1. Non-dissociation approach (NDA)

For the sake of simplicity, one first assumes that there is no species dissociation. Methods employing this assumption are included in textbooks [36–38]; they are briefly outlined here as they are necessary for the presentation of later work. For lean and stoichiometric conditions ($\phi \leq 1$), a common approach is to assume that all the fuel C and H react to forms of CO_2 and H_2O, respectively. CO and H_2 are thus not present in the combustion products and $\nu_2 = \nu_4 = 0$. $n_s = 0$ and it is not necessary to introduce any elementary reaction. The C-, H- and O-atom balance equations can be used to resolve the coefficients ν_k, as:

$$\begin{aligned} \nu_1 &= x & \nu_3 &= \frac{y}{2} \\ \nu_5 &= (1-\phi)a & \nu_t &= x + \frac{y}{2} + (4.76 - \phi)a \end{aligned} \tag{3}$$

where ν_t denotes the total mole number of products per mole of fuel. Mole fractions can be calculated as $X_k = \nu_k/\nu_t$. For rich mixing conditions $\phi > 1$, it is assumed that all the oxygen is consumed and none appears in the final products, so that $\nu_5 = 0$. One now has three equations but four unknowns. To close the system, the water-gas shift equilibrium equation is used, written as, $CO + H_2O \rightleftharpoons CO_2 + H_2$. The coefficients for rich flames are calculated as [37]:

$$\nu_1 = b = \frac{2a(K_{p,3}-1) + x + y/2}{2(K_{p,3}-1)} - \frac{1}{2(K_{p,3}-1)}\left[\left(2a(K_{p,3}-1) + x + y/2\right)^2 - 4K_{p,3}(K_{p,3}-1)(2ax - x^2)\right]^{1/2} \tag{4}$$

$$\begin{aligned} \nu_2 &= x - b & \nu_3 &= 2a - b - x \\ \nu_4 &= -2a + b + x + \frac{y}{2} & \nu_t &= x + \frac{y}{2} + 3.76a \end{aligned} \tag{5}$$

where $K_{p,3} = (\nu_1\nu_4)/(\nu_2\nu_3)$ is the equilibrium constant of the water-gas shift reaction. Note here that $K_{p,3} = K_{p,2}/K_{p,1}$. This method provides good estimates of the mole fractions of the combustion products when the flame temperature is not high, e.g., the fresh mixture is far from stoichiometric conditions. It can therefore be used to estimate the composition of lean mixtures; most combustion instabilities occur for lean flames [2]. It has been widely used to quickly estimate the mole fractions of combustion products and, when combined with the conservation of the standardised enthalpy, to estimate the adiabatic flame temperature (as in Section 3 of this work). However, when the flame temperature is high or the fresh mixture approaches stoichiometric conditions, dissociations cannot be neglected: CO and H_2 are present even in lean premixed flames and O_2 is present in rich flames.

2.2. Two dissociated species approach (TDSA)

We now consider that these six major species are always present in the final combustion products. The minimum number of elementary reactions is thus $n_e = 2$. To close the system, a commonly used approach is to assume an ε_1 amount of CO_2 and an ε_2 amount of H_2O dissociations, with their partial equilibrium equations $CO_2 \rightleftharpoons CO + 0.5O_2$ and $H_2O \rightleftharpoons H_2 + 0.5O_2$, respectively. The species coefficients are changed to [40]:

$$\begin{aligned} \nu_1 &= (1-\varepsilon_1)x & \nu_2 &= \varepsilon_1 x \\ \nu_3 &= \frac{(1-\varepsilon_2)y}{2} & \nu_4 &= \frac{\varepsilon_2 y}{2} \\ \nu_5 &= (1-\phi)a + \frac{\varepsilon_1 x}{2} + \frac{\varepsilon_2 y}{4} & \nu_t &= (1+\frac{\varepsilon_1}{2})x + (\frac{1}{2}+\frac{\varepsilon_2}{4})y + (4.76-\phi)a \end{aligned} \tag{6}$$

The values of ε_1 and ε_2 need to be simultaneously determined by the two partial equilibrium dissociation reactions with their equilibrium constants expressed as:

$$K_{p,1} = \frac{\nu_2}{\nu_1}\left(\frac{p}{p_0}\right)^{1/2}\left(\frac{\nu_5}{\nu_t}\right)^{1/2} = \frac{\varepsilon_1}{1-\varepsilon_1}\left(\frac{p}{p_0}\right)^{1/2}\left(\frac{\nu_5}{\nu_t}\right)^{1/2} \tag{7}$$

$$K_{p,2} = \frac{\nu_4}{\nu_2}\left(\frac{p}{p_0}\right)^{1/2}\left(\frac{\nu_5}{\nu_t}\right)^{1/2} = \frac{\varepsilon_2}{1-\varepsilon_2}\left(\frac{p}{p_0}\right)^{1/2}\left(\frac{\nu_5}{\nu_t}\right)^{1/2} \tag{8}$$

where p indicates local ambient pressure. $K_{p,1}$ and $K_{p,2}$ are the equilibrium constants of these two partial dissociation reactions, respectively. Species dissociations depend on the flow pressure and temperature. As ambient pressure increases, ε_1 and ε_2 decrease and less dissociations occur. By solving these two equations, the two variables, ε_1 and ε_2 can be found, giving the mixture composition of the products.

2.3. Simplified two dissociated species approach (STDSA)

The above method provides a good estimate of the mole fractions of hydrocarbon-air combustion products. However, these equations are complicated and solving these nonlinear algebraic equations is relatively costly for low order predictions of combustion instabilities or CFD simulations, especially when they are utilised in the calculation of flame temperature. A simplified approach, denoted *STDSA*, is proposed by combining the above two methods. Corrections deduced from the two dissociation equilibrium equations are added to the mixture composition obtained from the *NDA* method.

We now assume that amount ζ_1 of CO_2 dissociates to CO and O_2, and amount ζ_2 of H_2O dissociates to H_2 and O_2, based on the mixture composition from the *NDA* method. Denoting the mixture coefficients of these six major species from the *NDA* method by ν_k^*, the final corrected coefficients can thus be expressed as the superposition of basic values ν_k^* and corrections $\Delta\nu_k$, written as $\nu_k = \nu_k^* + \Delta\nu_k$. The corrections can be calculated as $\Delta\nu = [-\zeta_1, \zeta_1, -\zeta_2, \zeta_2, (\zeta_1 + \zeta_2)/2, 0]$. For lean and stoichiometric conditions, the basic values ν_k^* can be obtained from Eq. (3). Substitution of the final corrected coefficients ν_k into the expression of equilibrium constant $K_{p,1}$ (Eq. (7)) of the partial equilibrium equation of CO_2 dissociation, followed by linearisation about ν_k^*, leads to a simplified cubic function which contains only one unknown, ζ_1. The equation can be expressed as:

$$\zeta_1^3 + 2\nu_5^*\zeta_1^2 - 2\kappa = 0 \tag{9}$$

where the coefficient κ is related to the equilibrium coefficient, and is written as:

$$\kappa = (K_{p,1}\nu_1^*)^2\nu_t^*\frac{p_0}{p} \tag{10}$$

The solution can be expressed as:

$$\zeta_1 = \begin{cases} -\frac{2}{3}\nu_5^* + \left(\kappa - \frac{8}{27}\nu_5^{*3} + \left(\kappa^2 - \frac{16}{27}\kappa\nu_5^{*3}\right)^{1/2}\right)^{1/3} + \left(\kappa - \frac{8}{27}\nu_5^{*3} - \left(\kappa^2 - \frac{16}{27}\kappa\nu_5^{*3}\right)^{1/2}\right)^{1/3} & \text{if } \kappa \geq \frac{16}{27}\nu_5^{*3} \\ \frac{2}{3}\nu_5^*\left(2\cos\left(\arccos\left(\frac{27\kappa}{8\nu_5^{*3}} - 1\right)/3\right) - 1\right) & \text{if } \kappa < \frac{16}{27}\nu_5^{*3} \end{cases} \tag{11}$$

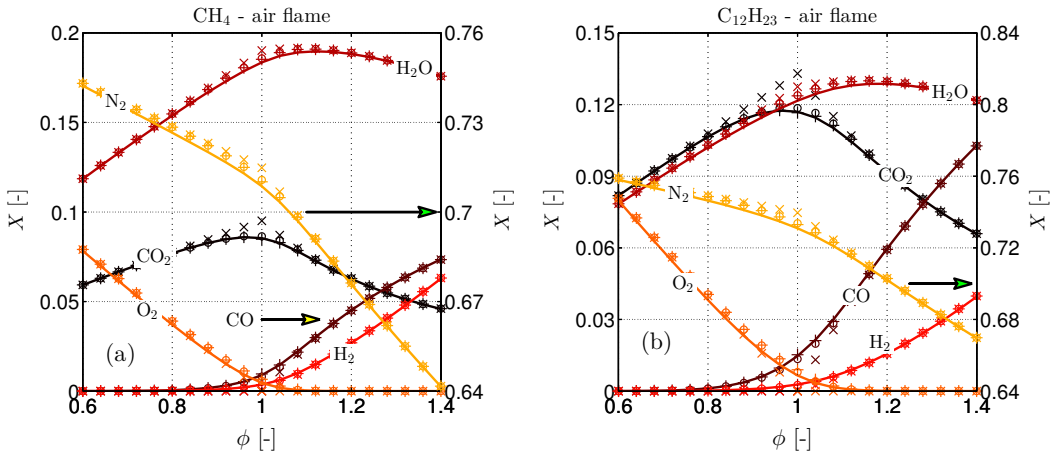

Figure 2: The mole fractions of the 6 major species in the combustion products of two hydrocarbon-air flames. Continuous lines: results calculated using the CANTERA code. Crosses ×: results calculated using *NDA*. Circles ○: results calculated using *TDSA*. Pluses +: results calculated using *STDSA*. The first 5 species correspond to the left axis and the species N_2 corresponds to the right axis.

$K_{p,1}$ increases with temperature, thus the corrections increase with temperature and decrease with ambient pressure. The coefficients ζ_1 and ζ_2 are connected by the water-gas shift equilibrium equation, which in simplified form can be written as:

$$\zeta_2 = \frac{K_{p,3}\nu_3^*}{\nu_1^*}\zeta_1 \tag{12}$$

These corrections change for rich flames, with the derivation method similar to that used for lean and stoichiometric flames. The basic values ν_k^* are calculated using Eq. (5). The coefficient ζ_1 can again be solved from a simplified cubic function, mathematically expressed as:

$$\zeta_1(\zeta_1 + \nu_2^*)^2 - 2\kappa = 0 \tag{13}$$

with the solution:

$$\zeta_1 = -\frac{2}{3}\nu_2^* + \left(\kappa + \frac{1}{27}\nu_2^{*3} + \left(\kappa^2 + \frac{2}{27}\kappa\nu_2^{*3}\right)^{1/2}\right)^{1/3} + \left(\kappa + \frac{1}{27}\nu_2^{*3} - \left(\kappa^2 + \frac{2}{27}\kappa\nu_2^{*3}\right)^{1/2}\right)^{1/3} \tag{14}$$

The correction coefficient ζ_2 is again considered to be proportional to ζ_1 with the same relation as Eq. (12). As presented above, the two dissociation amounts are decoupled and calculated separately. This method provides the explicit solution of the mixture composition of hydrocarbon-air combustion products and reduces the calculation cost compared to using coupled equations, as in the *TDSA* method.

Validation was carried out using two laminar premixed flames. The first uses methane CH_4 as a fuel, for which the ratio of mole number of H-atom to that of C-atom is large ($y/x = 4$ in the chemical formula). The second uses kerosene Jet-A (gas state) as a fuel, which has an equivalent chemical formula of $C_{12}H_{23}$. Tests were carried out with the fresh mixture at the state: $T_i = 300$ K and $p_i = 101325$ Pa, where T_i is the temperature of fresh mixture and p_i is the ambient pressure and is considered constant throughout the combustion. The results are compared with those computed using the CANTERA code [34] with the GRI-Mech 3.0 mechanism, comprising 325 elementary chemical reactions with associated rate coefficient expressions and thermochemical parameters for the 53 species. The adiabatic flame temperatures are also calculated using CANTERA and are then used to predict the mole fractions for each method. Figure 2 shows profiles of the mole fractions of 6 species with equivalence ratio ϕ calculated using the different methods. Results from all three methods, *NDA*, *TDSA* and *STDSA*, match the reference CANTERA results for very lean and very rich flames. When the mixture equivalence ratio ϕ approaches unity, the adiabatic flame temperature increases and dissociations cannot be neglected. The *NDA* predictions no longer match the reference results well: this difference increases with flame temperature. Both of the two dissociated species methods, *TDSA* and *STDSA* match the reference results, even for very high flame temperature. The simplification in *STDSA* does not result

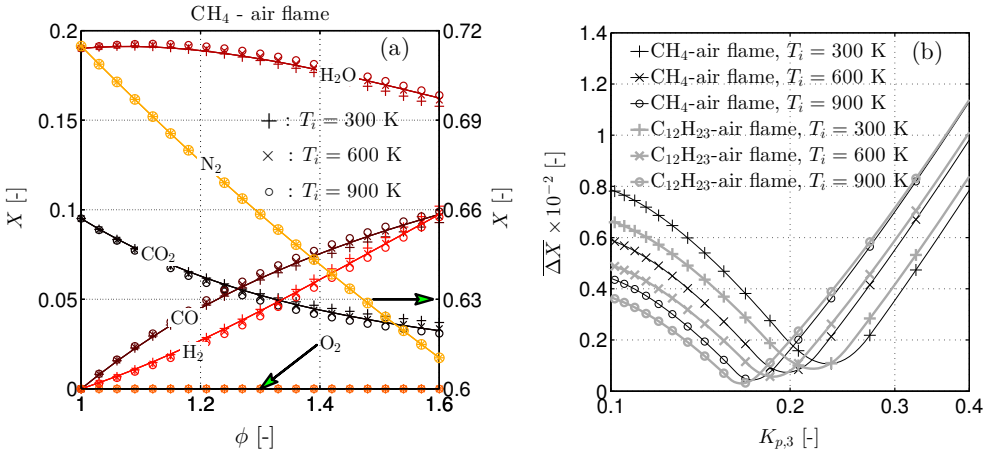

Figure 3: Left figure: calculation of the mole fractions X of six species for different fresh mixture temperatures T_i. Solid lines denote $K_{p,3}$ changing with temperature, and symbols denote constant $K_{p,3} = 0.2$. Right figure: calculation error $\overline{\Delta X}$ with $K_{p,3}$ for two flames at different fresh mixture temperatures, when $K_{p,3}$ is considered constant. ϕ ranges from 1.0 to 1.6 with step of 0.033.

in a loss of precision compared to *TDSA*. One can thus safely use the simplified method, *STDSA*, to quickly estimate the mole fractions of hydrocarbon-air combustion products. The *STDSA* method is also used in the following section to predict flame temperature.

3. Simplified flame temperature calculations

Prediction of thermoacoustic stability using low order modelling methods requires accurate knowledge of the temperature downstream of combustion – the "flame temperature". A simplified and efficient method for predicting this is now presented. The flame front can be treated as an interface separating the fresh unburned mixture and burned gases, which is extremely thin compared to the dominant acoustic wavelengths due to large activation energy [41–43]. Only the average flame temperature then needs to be known – there is no need to calculate the temperature profile around the flame front [44]. The flame temperature of the global reaction can be calculated using the following enthalpy balance equation for either "frozen" or equilibrium processes [36, 37]:

$$\eta\left(\Delta h^0_{f,\mathrm{C_xH_y}} - \sum_k \nu_k \Delta h^0_{f,k}\right) = \overbrace{\sum_k \nu_k \Delta h_{s,k}(T_f)}^{\text{combustion products}} - \overbrace{\left(\Delta h_{s,\mathrm{C_xH_y}}(T_i) + a\left(\Delta h_{s,\mathrm{O_2}}(T_i) + 3.76\Delta h_{s,\mathrm{N_2}}(T_i)\right)\right)}^{\text{fresh mixture}} \tag{15}$$

where T_i represents the temperature of fresh mixture and T_f stands for the flame temperature, which is to be determined. $\Delta h^0_{f,k}$ represents the standard enthalpy of formation per mole of species $\mathcal{M}_k$ at standard-state temperature $T_0 = 298.15$ K (e.g. Table 1 shows Δh^0_f for the 6 major species in burned gases and three often used fuels), $\Delta h_{s,k}(T) = \int_{T_0}^{T} C^m_{p,k}\mathrm{d}T$ stands for the difference of sensible enthalpy at temperature T compared to that at temperature T_0. $C^m_{p,k}$ represents the heat capacity at constant pressure per mole of species $\mathcal{M}_k$ and also depends on temperature. The components on the left side of Eq. (15) denote the enthalpy of formation at standard reference state and can be used as the heat release rate, which is not straightforward to measure [45–47], and is important for thermoacoustic analysis. Once the flame temperature is determined, the value of time-averaged heat release rate can thus also be obtained. The components on the right side of Eq. (15) represent the sensible enthalpy change of the reaction. η is the combustion efficiency empirically accounting for heat losses and imperfect combustion [39, 48]. The final temperature of the burned gases drops as combustion efficiency decreases. As presented in the previous section, the mole fractions of the mixture also change with temperature. When the temperature of the burned gases is low or mixture compositions are far from stoichiometric conditions, dissociations of species are weak and the temperature of burned

gases can be calculated in a straightforward manner by substituting mole fractions ν_k^* from the *NDA* method into Eq. (15).

The mole fractions of the 6 product species do not depend on temperature for lean and stoichiometric conditions. For rich flames they depend slightly on flame temperature, as the equilibrium coefficient $K_{p,3}$ of the water-gas shift equilibrium reaction changes with temperature, and iterations are necessary even for approximate prediction of the flame temperature. It is interesting to note that the mole fractions of burned gases calculated from Eqs. (4) and (5) are very similar to those obtained when $K_{p,3} \approx 0.2$ is assumed, for rich flames. Figure 3(a) compares the mole fractions X_k of six species for different fresh mixture temperatures (T_i = 300, 600 and 900 K) with those calculated assuming $K_{p,3} = 0.2$ for the CH_4-air flame. The difference can be evaluated by:

$$\overline{\Delta X} = \frac{1}{6}\sum_{k=1}^{6}\int_{\phi_1}^{\phi_2}\left|X_k - \check{X}_k\right|\mathrm{d}\phi \Big/ \int_{\phi_1}^{\phi_2}\mathrm{d}\phi \tag{16}$$

which is shown in Fig. 3(b) for CH_4-air and $C_{12}H_{23}$-air flames, at different fresh mixture temperatures T_i = 300, 600 and 900 K. $\check{X}_k$ denotes the mole fraction of species $\mathcal{M}_k$ when $K_{p,3}$ is chosen as a constant. The difference changes with $K_{p,3}$ and is weak when the equilibrium coefficient approaches 0.2. For the sake of simplicity, $K_{p,3} = 0.2$ is assumed in the prediction of flame temperature of rich hydrocarbon-air flames.

Table 1: Standard enthalpy of formation per mole of the major species in burned gases and three often used fuels Δh_f^0 (kJ mol^{-1}).

CO_2	CO	H_2O	H_2	O_2	N_2	CH_4	C_3H_8	$C_{12}H_{23}$
-393.510	-110.540	-241.826	0	0	0	-74.800	-104.680	-249.657

Table 2: Polynomial coefficients of degree 2 for 6 major species in burned gases and three fuels for two ranges of temperature: [300, 1000] K and [1000, 3000] K.

	$T \in [300, 1000]$ K				$T \in [1000, 3000]$ K			
	$\check{a}_2 \times 10^{-3}$	$\check{a}_1$	$\check{a}_0 \times 10^3$	Λ (%)	$\check{a}_2 \times 10^{-3}$	$\check{a}_1$	$\check{a}_0 \times 10^3$	Λ (%)
CO_2	11.6	32.9	-11.0	2.30	1.63	53.5	-22.0	0.12
CO	3.30	26.7	-8.19	0.55	0.85	32.6	-12.0	0.10
H_2O	5.75	29.5	-9.28	0.52	3.77	36.1	-14.3	0.21
H_2	0.69	28.5	-8.57	0.16	1.76	27.1	-8.25	0.07
O_2	4.28	26.9	-8.40	0.38	1.20	32.9	-11.5	0.02
N_2	2.91	26.7	-8.20	0.67	0.93	32.0	-11.7	0.10
CH_4	28.6	18.2	-8.0	0.51	9.27	63.0	-34.8	0.33
C_3H_8	71.0	41.1	-19.2	3.78	13.1	166.4	-89.7	0.32
$C_{12}H_{23}$	242.9	185.3	-78.9	3.28	44.2	609.4	-314.7	0.30

We now proceed to approximate prediction of flame temperature using mole fractions when species dissociations are neglected. Mole fractions are now constant for constant equivalence ratio of the fresh mixture ϕ. However, the difference of sensible enthalpy $\Delta h_s(T)$ varies with temperature and empirical fitted polynomials, such as NASA polynomial coefficients, are generally employed. For the species $\mathcal{M}_k$, $\Delta h_{s,k}(T)$ can be computed by:

$$\frac{\Delta h_{s,k}}{R} \approx \frac{\check{\Delta h}_{s,k}}{R} = -\frac{a_{k,1}}{T} + a_{k,2}\ln T + a_{k,3}T + \frac{a_{k,4}}{2}T^2 + \frac{a_{k,5}}{3}T^3 + \frac{a_{k,6}}{4}T^4 + \frac{a_{k,7}}{5}T^5 + b_{k,1} \tag{17}$$

The symbol ($\check{}$) represents the empirical fitted polynomial. $a_{k,n}$, $n = 1, \cdots 7$ and $b_{k,1}$ are polynomial coefficients of the species $\mathcal{M}_k$ and are available in the GRI-MECH 3.0 database (see the NASA Glenn Research Center website

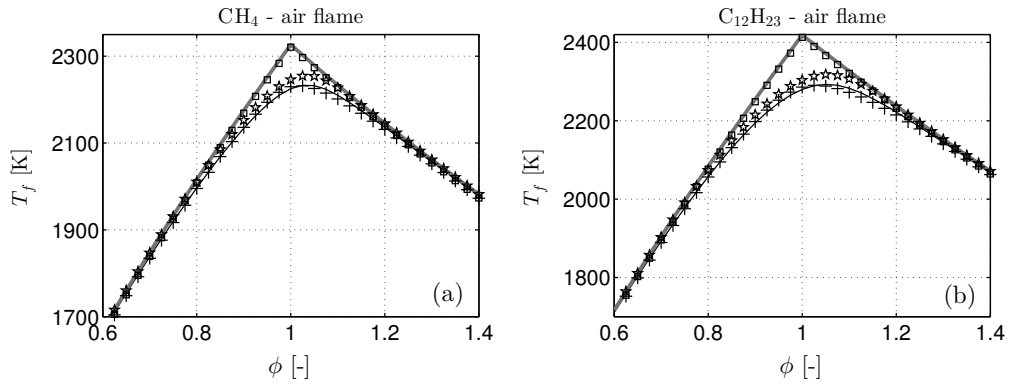

Figure 4: Adiabatic flame temperature distribution with equivalence ratio of the fresh mixture calculated using different methods. $\eta = 1$. The temperature of the fresh mixture equals $T_i = 300$ K. The ambient pressure $p_i = 1$ Bar. Gray thick continuous lines: results calculated using *NDA* using NASA polynomial coefficients and $K_{p,3}$ changing with temperature. Black thin continuous lines: results calculated using the Cantera code. Boxes □: results calculated using *NDA* using proposed 2 degree polynomial coefficients with $K_{p,3} = 0.2$ for rich flames. Stars ⋆: results calculated using *TDSA*. Pluses +: results calculated using *STDSA*.

`http://www.grc.nasa.gov/WWW/CEAWeb/ceaHome.htm`). It is also possible to compute the heat capacity per mole at constant pressure $C^m_{p,k}$, written as:

$$\frac{C^m_{p,k}}{R} = \frac{1}{R}\Big(\frac{\partial h_{s,k}}{\partial T}\Big)_p \approx \frac{a_{k,1}}{T^2} + \frac{a_{k,2}}{T} + a_{k,3} + a_{k,4}T + a_{k,5}T^2 + a_{k,6}T^3 + a_{k,7}T^4 \tag{18}$$

These polynomials provide good estimation of $\Delta h_s(T)$. The flame temperature can then be calculated by combining them with mole fractions from the *NDA* method. The calculation can be further simplified using lower degree polynomials. Table 2 shows the polynomials of degree 2 for the 6 major species in the burned gases and three fuels for two temperature ranges, [300,1000] K and [1000, 3000] K. $\Delta h_s(T)$ now can be computed as:

$$\Delta h_s(T) \approx \Delta \check{h}_s(T) = \check{a}_2 T^2 + \check{a}_1 T + \check{a}_0 \tag{19}$$

The fitting error can be evaluated using:

$$\Lambda = \int_{T_1}^{T_2} \left|\Delta h_s(T) - \Delta \check{h}_s(T)\right| \mathrm{d}T \Big/ \int_{T_1}^{T_2} \Delta h_s(T) \mathrm{d}T \tag{20}$$

where T_1 and T_2 are the lower and upper limits of the fitting temperature range, respectively. It should be highlighted that unlike for the high degree polynomials used in the NASA database, the heat capacity per mole at constant pressure $C^m_p(T) = \partial \Delta_s(T)/\partial T$ cannot be calculated precisely from these polynomial coefficients – they are only used to predict the flame temperature. The fitting errors are generally very small, except for those of CO_2, C_3H_8 and $C_{12}H_{23}$ at lower temperatures, although calculations show that these errors have little effect on the final predicted flame temperature. Figures 4, 5 and 6 show the adiabatic flame temperature calculated using (1) the *NDA* method with NASA polynomial coefficients and $K_{p,3}$ varying with temperature, and (2) the *NDA* method using the 2 degree polynomial coefficients and $K_{p,3} = 0.2$. Different flames, fresh mixture temperatures T_i and ambient pressures p_i are considered. The differences are very small. It is thus possible to use the simplified method to predict the flame temperature when species dissociations are weak.

One now progresses to precise prediction of the flame temperature. When accounting for 6 species, flame temperatures are often calculated by combining mole fractions deduced from Eqs (6), (7) and (8) and the enthalpy balance equation Eq. (15). For consistent notation, this flame temperature calculation method is therefore named *TDSA* as well.

The dissociation amounts of CO_2 and H_2O are coupled and also depend on the flame temperature – the calculation is complicated. The *STDSA* method shown in Section 2.3 can be used to simplify the calculation. Corrections are

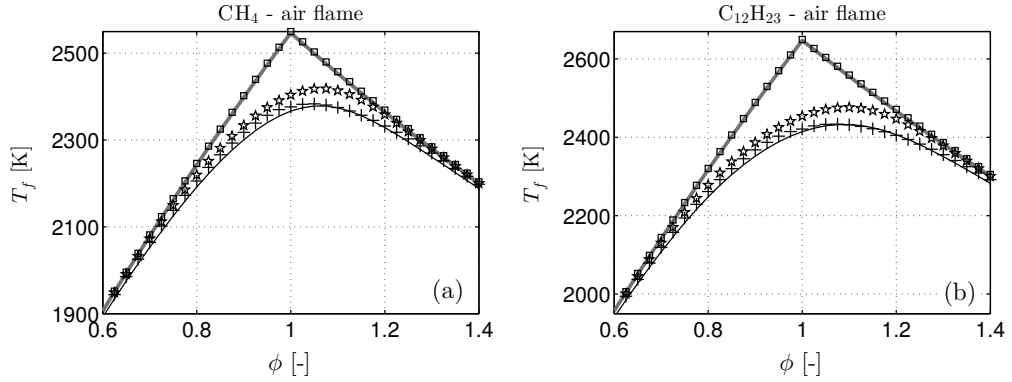

Figure 5: Adiabatic flame temperature distribution with equivalence ratio of the fresh mixture calculated using different methods. $\eta = 1$. The temperature of the fresh mixture equals $T_i = 600$ K. The ambient pressure $p_i = 1$ Bar. See the caption of Fig. 4 for the representation of the markers.

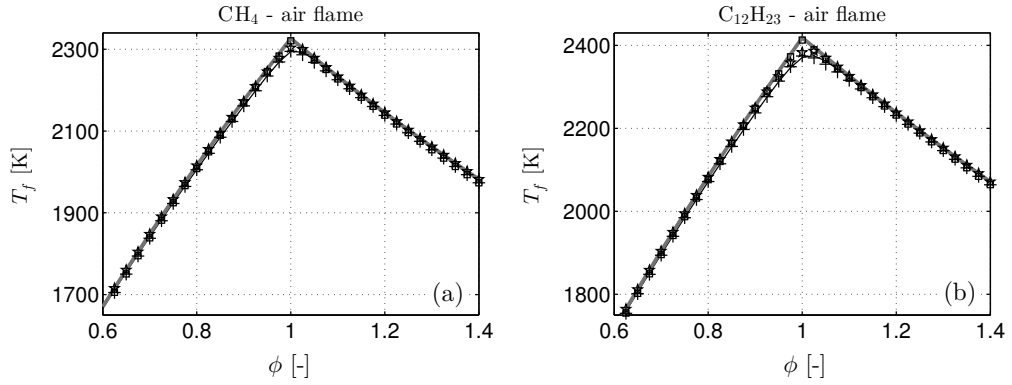

Figure 6: Adiabatic flame temperature distribution with equivalence ratio of the fresh mixture calculated using different methods. $\eta = 1$. The temperature of the fresh mixture equals $T_i = 300$ K. The ambient pressure $p_i = 100$ Bar. See the caption of Fig. 4 for the representation of the markers.

based on the *NDA* results. Denoting mixture coefficients from the *NDA* method by ν_k^*, the final corrected coefficients can thus be expressed as the superposition of basic values ν_k^* and corrections $\Delta\nu_k$, written as $\nu_k = \nu_k^* + \Delta\nu_k$. We can also represent the flame temperature from the *NDA* method as T_f^* and the correction as ΔT_f. Since $\Delta\nu_k \ll \nu_k^*$ and $\Delta T_f \ll T_f^*$, Eq. (15) can be linearised as:

$$\sum_k \left(\Delta\nu_k \left(\Delta h_{s,k}(T_f^*) + \eta\Delta h_{f,k}^0\right) + \nu_k^* C_{p,k}^m(T_f^*)\Delta T_f\right) = 0 \tag{21}$$

Corrections in coefficients of species can be expressed as $\Delta\nu = [-\zeta_1, \zeta_1, -\zeta_2, \zeta_2, (\zeta_1 + \zeta_2)/2, 0]$, where the coefficients ζ_1 and ζ_2 can be calculated using Eqs. (11) and (12) for lean and stoichiometric flames and using Eqs. (14) and (12) for rich flames. Substituting $\Delta\nu$ into Eq. (21) and making further simplification and approximation, one obtains the expression for lean and stoichiometric flames:

$$\eta\left(\alpha_1 + \alpha_2\frac{y}{2x}\right)\frac{3\beta + 2\nu_5^*}{3\beta + 4\nu_5^*}\beta + \sum_{k=1}^{6}\nu_k^*\left(2\breve{a}_{k,2}T_f^* + \breve{a}_{k,1}\right)\Delta T_f = 0 \tag{22}$$

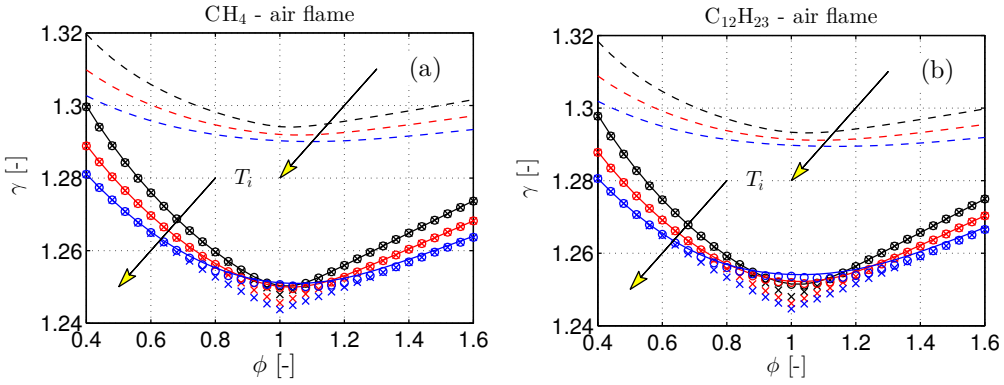

Figure 7: Ratio of specific heats of combustion products, γ, against mixture equivalence ratio, ϕ, for different fresh mixture temperatures T_i of 300 K (black), 600 K (red) and 900 K (blue). Flames are adiabatic and isobaric. Continuous lines: results calculated using the CANTERA code. Crosses ×: results using *NDA*. Circles ○: results using *STDSA*. Dashed lines: γ of air at corresponding temperature.

where $\alpha_1 = 2.78 \times 10^5$, $\alpha_2 = 5.02 \times 10^4$. β is the function of ΔT_f and can be expressed as:

$$\beta = \left(2\nu_t^*(\nu_1^*)^2 \frac{p_0}{p}\right)^{1/3} \exp\left(\frac{56}{R} - \frac{1.86 \times 10^5}{RT_f^*}\right) \exp\left(\frac{1.86 \times 10^5}{RT_f^{*2}} \Delta T_f\right) \tag{23}$$

The values of $\check{a}_{k,n}$ are shown in Table 2. Eq. (22) only has one unknown ΔT_f and is straightforward to solve. For rich flames, Eq. (22) becomes:

$$\eta\left(\alpha_1 + \alpha_2 \frac{y}{2x}\right) \frac{2\beta^2}{2\beta + \nu_2^*} + \sum_{k=1}^{6} \nu_k^* \left(2\check{a}_{k,2} T_f^* + \check{a}_{k,1}\right) \Delta T_f = 0 \tag{24}$$

To validate the method, CH_4-air and $C_{12}H_{24}$-air flames are considered. Figures 4, 5 and 6 show the comparisons between results from the proposed method (*STDSA*), reference results from the CANTERA code and results from the *TDSA* method. Compared to the *TDSA* method, results from the proposed *STDSA* method match the reference results better. At high temperature, more species dissociate and the real flame temperature is generally lower than that predicted by the two dissociated species methods [36]. The reason for the better prediction by the proposed method is the neglected high order terms in Eq. (21). Validation using other fuels and operating conditions confirmed that the proposed *STDSA* method always predicts the flame temperature accurately and is a reliable and efficient method of computing the flame temperature.

4. Simplified calculation of the ratio of specific heats and speed of sound in the combustion products

For prediction of thermoacoustic stability using low order methods, both the time-averaged ratio of specific heats and speed of sound in hydrocarbon-air combustion products must be known accurately. One now progresses to calculation of these. The heat capacity per mole at constant pressure for a "frozen" or equilibrium mixture can be expressed as:

$$C_p^m(T) = \sum_k X_k(p, T, \phi) C_{p,k}^m(T) \tag{25}$$

where X_k denotes the mole fraction of the species $\mathcal{M}_k$ and changes with temperature and pressure, as presented in Section 2. $C_{p,k}^m(T)$ represents the heat capacity at constant pressure for the species $\mathcal{M}_k$. It changes with temperature and cannot be considered constant for large changes in combustion chamber temperature. In most hydrocarbon-air flames, the nitrogen species dominates and the heat capacity of the mixture is close to that of nitrogen and air. The heat capacity of the mixture has always previously been treated as that of air, or considered a constant [29, 43]. A

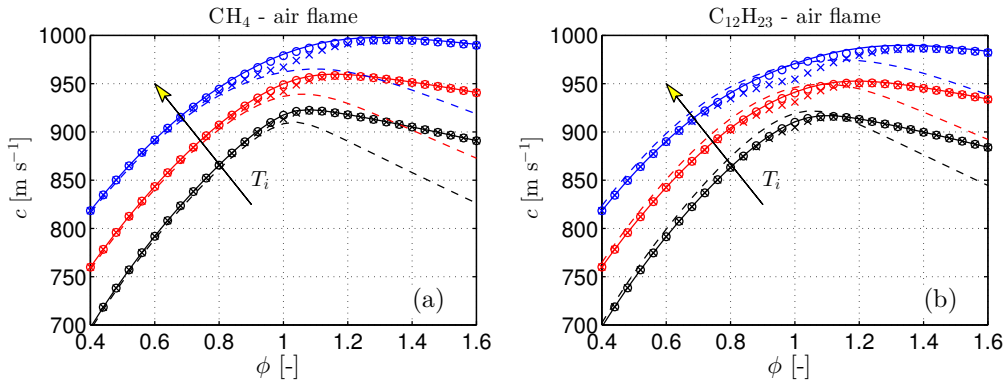

Figure 8: Speed of sound, c, in the combustion products against mixture equivalence ratio, ϕ, for different fresh mixture temperatures T_i of 300 K (black), 600 K (red) and 900 K (blue). Flames are adiabatic and isobaric. See the caption of Fig. 7 for the representation of the markers.

temperature change from 300 K to 3000 K results in air heat capacity changes of around 30% [24]. It therefore follows that these simplifications may introduce errors to the prediction of thermoacoustic modes. In this work, the effect of neglecting detailed changes in the heat capacity of the mixture is investigated, by taking advantage of the simplified method of calculating mole fractions presented in Section 2. The ratio of specific heats of the mixture can be written as:

$$\gamma = \frac{C_p^m}{C_p^m - R} \tag{26}$$

which also varies with temperature and mixture composition.

Assuming that the reaction time or mixing time of combustion products with diluted gases (such as air) is sufficiently small, the flow can be considered "frozen" or in equilibrium. The speed of sound of the mixture can be calculated using [38, 49]:

$$c = \left(\frac{\partial p}{\partial \rho}\right)_{s,X_k} = \left(\gamma \frac{R}{W} T\right)^{1/2} = \left(\frac{C_p^m}{C_p^m - R} \frac{R}{W} T\right)^{1/2} \tag{27}$$

with the mixture molecular weight W:

$$W = \sum_k X_k W_k \tag{28}$$

It is now interesting to examine the ratio of specific heats γ and speed of sound c in the combustion products as computed using the *TDSA* and *STDSA* methods. Validation is again carried out using methane CH_4 and kerosene Jet-A $C_{12}H_{23}$ flames. The flame temperature for the *STDSA* method is computed using the method proposed in Section 3. All other flame temperatures are calculated using the CANTERA code.

Figure 7 shows how the ratio of specific heats, γ, varies with the equivalence ratio of the fresh mixture for the different calculation methods. The variations of γ_{air} with equivalence ratio at the different temperatures are also shown for comparison. The ratios clearly vary with temperature and cannot be considered to be a constant 1.4. Furthermore, the difference between the ratio for air and for the combustion products cannot be neglected, especially for stoichiometric flames. The *STDSA* method predicts the variation well, particularly for high temperature conditions.

Comparisons of the speed of sound c with equivalence ratio according to the different methods are shown in Fig. 8 along with the speed of sound for air. The proposed *STDSA* method provides a very good estimation of the speed of sound in the combustion products across different mixtures and operating conditions. Furthermore, the speed of sound for lean and stoichiometric combustion products is close to that for air at the corresponding temperature. This can be explained as follows.

As the heat capacities per mole at constant pressure C_p^m of the species CO, H_2, O_2 and N_2 are close to those of air,

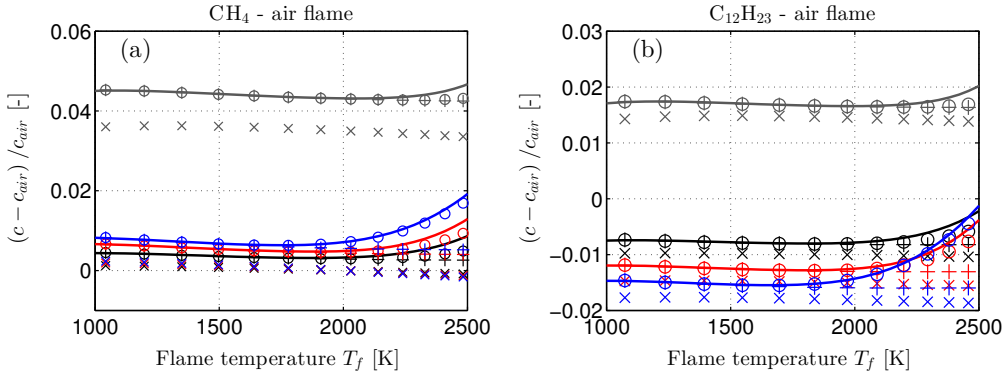

Figure 9: Ratio $(c - c_{air})/c_{air}$ against flame temperature T_f for different equivalence ratios ϕ. Continuous lines: results calculated using the CANTERA code. Crosses ×: results calculated using Eqs. (29) and (30). Circles ∘: results calculated using the *STDSA* method. Pluses +: results calculated using the *NDA* method. Black markers: $\phi = 0.5$. Red markers: $\phi = 0.8$. Blue markers: $\phi = 1.0$. Gray markers: $\phi = 1.3$.

C_p^m of the hydrocarbon-air combustion products can be simplified to:

$$C_p^m = C_{p,air}^m + \Delta C_p^m \approx \left(1 + 0.655\frac{\nu_1}{\nu_t} + (0.1 + 1.6 \times 10^{-4} T_f)\frac{\nu_3}{\nu_t}\right) C_{p,air}^m \quad \text{for } T_f \in [1000, 2000]K \tag{29}$$

where the coefficient ν_k of species $\mathcal{M}_k$ can be obtained using Eqs. (3), (4) and (5) or the *STDSA* method. It has been found that this approximation provides very good predictions for the flame temperature in the temperature range 1000 K to 2000 K for different operating and mixture conditions. This expression also provides a fast method of evaluating both C_p^m and γ for hydrocarbon-air combustion products for a given mixture equivalence ratio ϕ.

The speed of sound of the combustion products is related to that of air by:

$$c \approx \left(1 - \frac{\gamma_{air} - 1}{2}\frac{\Delta C_p^m}{C_{p,air}^m} - \frac{\Delta W}{2W_{air}}\right) c_{air} \tag{30}$$

where, the molecular weight W of the mixture is linked to that of air by, $W = W_{air} + \Delta W$, with the ratio $\Delta W/W_{air}$ calculated using:

$$\frac{\Delta W}{W_{air}} = \frac{0.416x - 0.2155y}{x + y/2 + (4.76 - \phi)a} \qquad \text{for } \phi \leq 1 \tag{31}$$

It is now straightforward to evaluate the difference between the speed of sound in the combustion products to that in air for lean and stoichiometric conditions. For lean and stoichiometric methane-air flames, the ratio of the mole number of H-atoms to that of C-atoms in the chemical formula has a large number, $y/x = 4$. The difference between the speed of sound in the combustion products and air $\Delta c/c_{air}$ equals to $2.45 \times 10^{-4}\phi/(9.52 + \phi)$ when $T_f = 2000$ K, and $-2.55 \times 10^{-2}\phi/(9.52 + \phi)$ when $T_f = 1000$ K. These values are very small compared to unity, hence the difference between the speed of sound in lean and stoichiometric methane-air flames and that in air can be neglected. When the ratio of y/x is reduced, e.g., $C_{12}H_{23}$, for kerosene-air flames, $\Delta c/c_{air}$ equals to $-0.335\phi/(14.86 + \phi)$ when $T_f = 2000$ K, and $-0.323\phi/(14.86 + \phi)$ when $T_f = 1000$ K. Again the difference between the speed of sound in lean and stoichiometric kerosene-air combustion products and air is small and can be neglected. The same results can be obtained by analysing equation (30). Compared to air, the combustion products have a larger heat capacity and smaller molecular weight [24], which in turn makes the speed of sound close to that in air. For rich flames, more species are present in the mixture and the effect of the molecular weight decrease is larger. The speed of sound in the combustion products thus cannot be evaluated by approximating to that of air at the corresponding temperature. This break down in the air-combustion product simplification is also validated by the results shown in Fig. 9. The simplified *STDSA* calculation models for calculating mole fractions, flame temperature, ratio of specific heats and speed of sound are now applied to thermoacoustic analysis of simple combustors in the following sections.

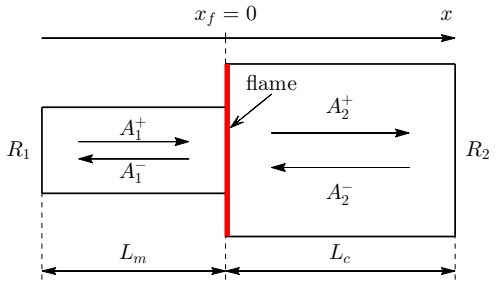

Figure 10: The sketch of the simplified combustor. The flame is located at $x = x_f = 0$. The lengths of the mixing section and combustion chambers are L_m and L_c respectively. Note that the subscripts m and c are used to represent the mixing section and combustion chamber respectively in the rest of the paper.

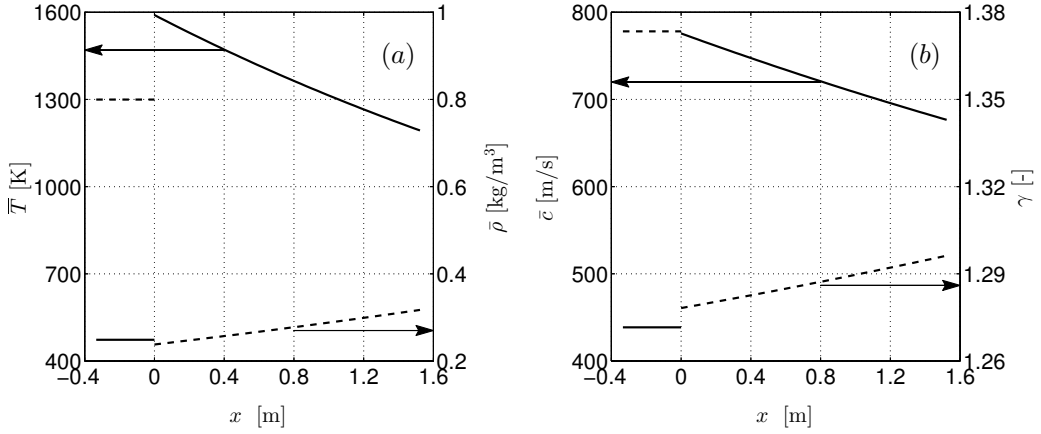

Figure 11: (a): evolutions of the time-averaged gas temperature $\overline{T}$ (represented by continuous lines and corresponding to the left y axis) and time-averaged gas density $\bar{\rho}$ (represented by dashed lines and corresponding to the right y axis) with locations x. (b): evolutions of the time-averaged speed of sound $\bar{c}$ in the gas (represented by continuous lines and corresponding to the left y axis) and ratio of specific heats γ (represented by dashed lines and corresponding to the right y axis) with locations x.

5. Application to the thermoacoustic analysis of a combustor with an axial temperature distribution

Low-order thermoacoustic network tools have been widely used in the prediction and analysis of thermoacoustic instabilities [20, 29, 50–52]. They represent the combustor and its attached components as a network of simple connected acoustic modules, where each module corresponds to a certain component of the system. The acoustic wave behaviour is modelled analytically using linear wave-based methods, and are combined with a flame model, which captures how the heat release rate responds to the acoustic waves [22, 30, 53]. This coupled approach has been successfully used to predict the thermoacoustic modal frequencies and growth rates of experimental lognitudinal combustors [22, 30]. In the configurations considered thus far, the combustion chamber lengths are short, such that their time-averaged thermodynamic properties can be considered uniform in space. However, for long combustion chambers, changes in the time-averaged gas temperature, $\overline{T}$, with axial distance may not be negligible. Then, the speed of sound, $\bar{c}$, ratio of specific heats, γ, and time-averaged density $\bar{\rho}$, all also change with axial location. Furthermore, species dissociations occur at high temperature, making the calculation of the distributions of these properties more complicated still. The methods presented in the previous sections are now used to accurately and efficiently calculate the axial profiles of these properties for a well-documented combustor comprising a long combustion chamber. These thermodynamic properties are then substituted into three low-order thermoacoustic analysis methods, in order to demonstrate the improved modal frequencies and growth rates predicted when spatial variations in properties are accounted for.

The present study focusses on a well documented experimental premixed combustor at Pennsylvania State Uni-

versity, which benefits from a variety of combustion instabilities studies [31, 54]. The combustor geometry can be simplified to two connected ducts, a mixing section and a variable-length combustion chamber, shown schematically in Fig. 10. The mixing section is $L_m = 333.5$ mm long and has an annular cross-section bounded by a 19.1 mm outer diameter centerbody and a 38.1 mm inner diameter mixing tube. The dominant acoustic wavelength is sufficiently larger than the mean diameter of the annular duct and only longitudinal acoustic waves propagate, which in turn enables the representation of the annular duct by a circular duct with equivalent diameter $d_m = 33.0$ mm, as shown in Fig. 10. The combustion chamber is also a circular duct with a $d_c = 109.2$ mm inner diameter, whose length, L_c, can be varied continuously from 762 mm to 1524 mm [31]. Denoting distance along the combustor axis by x, the entrance and end of the combustion chamber are at $x = x_f = 0$ and $x = L_c$, respectively. Methane and air are premixed in the mixing section with equivalence ratio $\phi = 0.6$, and a swirling flame is stabilised at the combustion chamber entrance. The time-averaged pressure throughout the combustor is considered constant at $\bar{p} = 112000$ Pa, with the mean flow velocity in the mixing section $\overline{u}_1 = 70$ m/s. The time-averaged temperature of the fresh mixture in the mixing section is considered uniform at $\overline{T}_1 = 473$ K; the flame temperature used in [31] is $\overline{T}_2 = 1591$ K, which is consistent with the predicted temperature by setting the combustion efficiency $\eta = 0.827$ using the *STDSA* method. The time-averaged temperature at the end of the combustion chamber is $\overline{T}_3 = 1193$ K when the combustion chamber length is $L_{c,max} = 1524$ mm; the time-averaged temperature profile with axial distance is unknown.

In the current work, we assume that heat losses are mainly from the heat transfer between the burned gases and combustion chamber wall. The heat transfer coefficient is assumed constant, implying a time-averaged temperature profile with an exponential spatial form [55]:

$$\overline{T}(x) = (\overline{T}_2 - \overline{T}_0)\exp(-\vartheta x) + \overline{T}_0, \qquad x_f^+ \le x \le L_{c,max} \quad \text{where} \quad \vartheta = \frac{1}{L_{c,max}} \ln\left(\frac{\overline{T}_2 - \overline{T}_0}{\overline{T}_3 - \overline{T}_0}\right) \tag{32}$$

where $\overline{T}_0$ is the ambient temperature and equals 293 K. Although this expression is obtained by assuming the ratio of specific heats γ and heat transfer coefficient constant in [55], it provides a simple and reasonable estimate of the temperature profile in a duct with a constant cross-sectional surface area. The resulting time-averaged temperature profile is shown in Fig. 11(a). By substituting this into the methods presented in previous sections, the profiles of the time-averaged density $\bar{\rho}(x)$, speed of sound $\bar{c}(x)$ and ratio of specific heats γ, can be predicted, as shown in Fig. 11(a) and (b).

The unsteady heat release rate of the flame can be related to the incoming acoustic velocity perturbations using a flame transfer function:

$$\mathcal{F}(\omega) = \frac{\widehat{\dot{Q}}/\overline{\dot{Q}}}{\hat{u}(x_f^-)/\bar{u}(x_f^-)} \tag{33}$$

where $\overline{\dot{Q}}$ is the time-averaged heat release rate and equals 73.49 kW [31]. Fig. 12 shows the experimentally measured flame transfer function under the assumption that the flame is "compact" (it is also called "global" flame transfer function in [31]) and can be assumed infinitely thin compared to the acoustic wavelength. Fitting to the experimental results is also shown; note that the previously used fitting expression[31] was not provided; the present work uses an improved fitting of order 6 in the thermoacoustic predictions.

Two low order wave-based methods are now used to predict the dominant thermoacoustic frequency and corresponding growth rate of the combustion system. They are compared to predictions obtained from a linearised Euler equation simulation, which acts as a reference check. The first low order method assumes constant thermodynamic properties within the combustion chamber, as used in [31], while the second accounts for the distributions of thermodynamic properties using the methods developed.

5.1. Reference prediction of main thermoacoustic mode using the linearised Euler equations (LEE)

The flow is taken to comprise a steady uniform time-averaged flow (denoted $\overline{()}$) and small perturbations (denoted $()'$). The mean flow speed is assumed negligible, and harmonic time variations are assumed for which all fluctuating variables have the form $a' = \hat{a}e^{i\omega t}$. Neglecting viscous terms and linearising the governing flow conservation equations then yields the linearised Euler equations (LEE) for the acoustic velocity and pressure perturbations [24]:

$$i\omega\hat{u} + \frac{1}{\overline{\rho}}\frac{\partial\hat{p}}{\partial x} = 0 \tag{34}$$

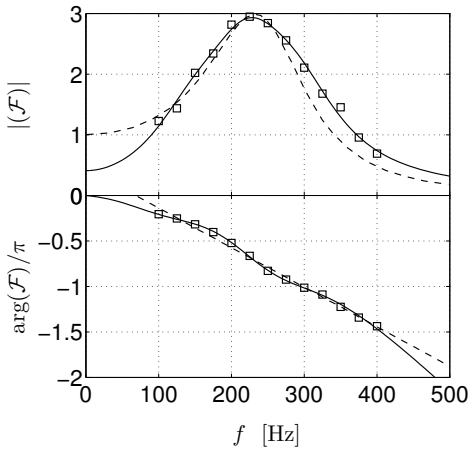

Figure 12: Evolutions of the gain (up figure) and phase (bottom figure) of the flame transfer function $\mathcal{F}$ with frequency f. Markers □: experimental results. Dashed lines: previous fitted flame transfer function [31]. Continuous lines: current fitted flame transfer function.

$$\frac{i\omega\hat{p}}{\gamma\bar{p}} + \frac{1}{S}\frac{\partial(S\,\hat{u})}{\partial x} = \frac{\gamma-1}{\gamma\bar{p}}\frac{\widehat{\dot{Q}}}{S} \tag{35}$$

where S is the cross-sectional surface area and $\widehat{\dot{Q}}$ is the unsteady heat release rate, which is zero away from the flame zone. Assuming a compact flame and integrating Eqs. (34) and (35) across the thin flame yields:

$$\hat{p}(x_f^+) = \hat{p}(x_f^-) \tag{36}$$

$$\hat{u}(x_f^+) - \frac{S_c}{S_m}\hat{u}(x_f^-) = \frac{\gamma-1}{\gamma\bar{p}}\frac{\widehat{\dot{Q}}}{S_m} \tag{37}$$

The pressure reflection coefficient at the entrance of the mixing section has been measured as $R_1 = 0.2292 - i0.1894$ [31], which enables the link between pressure and velocity perturbation terms at the entrance ($x = -L_m$):

$$\frac{R_1+1}{R_1-1}\bar{\rho}\bar{c}\hat{u} - \hat{p} = 0 \tag{38}$$

The outlet of the combustion chamber is a rigid wall; the velocity perturbation is thus $\hat{u}(L_c) = 0$ and the pressure reflection coefficient $R_2 = 1$. Combining Eqs. (34)-(35) for non-reacting flows, the jump conditions (Eqs. (36) and (37)), and the boundary conditions, one obtains an eigen-problem of the form:

$$\mathscr{A}\mathcal{V} = i\omega\mathcal{V} \tag{39}$$

where the matrix $\mathscr{A}$ is a linear operator applied to the eigenvector $\mathcal{V} = [\hat{p}, \hat{u}]^T$, and $\omega = \omega_r - i\sigma$ is a complex-valued eigenvalue of the system. Eigenvalues correspond to thermoacoustic modes with angular frequency $\omega_r = 2\pi f$ and growth rate σ, the stability of the mode being determined by the sign of the latter, with a positive value corresponding to an unstable system.

The central finite difference method and the staggered grid method [56] are used for the 1-D spatial discretisation. The operator $\mathscr{A}$ depends on ω via the flame transfer function and the Matlab command 'fsolve' is used to solve the nonlinear eigen-problem. Provided small enough discretisation steps are used, the results from the LEE method are taken as a reference calculation, fully accounting for spatial variation in thermodynamic properties.

5.2. Low order thermoacoustic model prediction assuming constant chamber properties

In a duct with a constant cross-sectional surface area, negligible mean flow speed and away from any heat sources, Eqs. (34) and (35), can be combined to give an equation with only one unsteady term $\hat{p}$:

$$\frac{\mathrm{d}^2\hat{p}}{\mathrm{d}x^2} - \frac{1}{\bar{\rho}}\frac{\partial\bar{\rho}}{\partial x}\frac{\mathrm{d}\hat{p}}{\mathrm{d}x} + \frac{\omega^2}{\bar{c}^2}\hat{p} = 0 \tag{40}$$

In the mixing section, the time-averaged thermodynamic properties are assumed uniform, hence $\partial\bar{\rho}/\partial x = 0$, and the solution to Eqs. (40) and (34), can be expressed analytically as the superposition of forward and backward propagating plane waves [57]:

$$\hat{p}(x) = A_1^+ \exp\left(-i\omega\frac{x+L_m}{\bar{c}_1}\right) + A_1^- \exp\left(i\omega\frac{x+L_m}{\bar{c}_1}\right) \tag{41}$$

$$\hat{u}(x) = \frac{1}{\bar{\rho}_1\bar{c}_1}\left(A_1^+ \exp\left(-i\omega\frac{x+L_m}{\bar{c}_1}\right) - A_1^- \exp\left(i\omega\frac{x+L_m}{\bar{c}_1}\right)\right), \qquad -L_m \le x \le x_f^- \tag{42}$$

where $A_1^{\pm}$ are the strengths of downstream/upstream propagating pressure waves and $\bar{\rho}_1$ and $\bar{c}_1$ are the time-averaged density and speed of sound, respectively.

The method that used previously[31] was to assume a uniform time-averaged temperature within the combustor, equal to the average value $\overline{T}^*$. The pressure and velocity perturbations then take the analytical form of plane wave propagating in either direction:

$$\hat{p}(x) = A_2^+ \exp\left(-i\omega\frac{x-x_f^+}{\bar{c}*}\right) + A_2^- \exp\left(i\omega\frac{x-x_f^+}{\bar{c}*}\right) \tag{43}$$

$$\hat{u}(x) = \frac{1}{\bar{\rho}_2^*\bar{c}_2^*}\left(A_2^+ \exp\left(-i\omega\frac{x-x_f^+}{\bar{c}*}\right) - A_2^- \exp\left(i\omega\frac{x-x_f^+}{\bar{c}*}\right)\right), \qquad x_f^+ \le x \le L_{c,max} \tag{44}$$

where $A_2^{\pm}$ are the strengths of the downstream/upstream propagating pressure waves. $\bar{c}^*$ and $\bar{\rho}^*$ are the average speed of sound and time-averaged density, respectively, here given by $\overline{T}^* = 1330$ K, $\bar{c}^* = 710.0$ m/s and $\bar{\rho}^* = 0.2582$ kg/m^3 [31]. By substituting Eqs. (41), (42), (43) and (44) into the jump conditions (Eqs. (36) and (37)), and combining with the flame transfer function (Eq. (33)) and the boundary conditions at the two ends, the acoustic wave strengths before and after the flame are found to satisfy:

$$\underbrace{\begin{bmatrix} 1 & -R_1 & 0 & 0 \\ e^{-i\omega L_m/\bar{c}_1} & e^{i\omega L_m/\bar{c}_1} & -1 & -1 \\ \Xi_1(1+\mathscr{Q}\mathscr{F}(\omega))e^{-i\omega L_m/\bar{c}_1} & -\Xi_1(1+\mathscr{Q}\mathscr{F}(\omega))e^{i\omega L_m/\bar{c}_1} & -1 & 1 \\ 0 & 0 & e^{-2i\omega L_c/\bar{c}^*} & -1 \end{bmatrix}}_{\mathbf{M_1}} \underbrace{\begin{bmatrix} A_1^+ \\ A_1^- \\ A_2^+ \\ A_2^- \end{bmatrix}}_{\mathscr{A}} = \mathbf{0} \tag{45}$$

where $\Xi_1 = (S_m/S_c)(\bar{\rho}^*\bar{c}^*)/(\bar{\rho}_1\bar{c}_1)$ and $\mathscr{Q} = (\gamma_1 - 1)\overline{\dot{Q}}/(\bar{\rho}_1\bar{u}_1\bar{c}_1^2 S_m)$. The eigenvalues of the system ω, obtained by solving the dispersion relation $det(M_1) = 0$, where det is the matrix determinant, give the thermoacoustic modes. The evolution of the first longitudinal mode frequency and growth rate with the length of the combustion chamber, L_c, are shown in Figure 13, along with experimental frequency measurements for unstable cases. The difference between the current and previous predictions with the global flame transfer function is simply due to the different fitting expressions for the transfer function used.

At this stage, it is worth noting that significant differences exist between the measured and predicted combustor lengths for which the mode is unstable (positive growth rate), and even for the modal frequency. In [31], this was attributed to the "compact flame" assumption; the flame length of around 150 mm is quite long and cannot be considered compact. The use of a distributed flame transfer function improved the prediction, but with still quite large differences. Unfortunately, the distributed flame transfer function was not provided in [31]. The present work therefore focusses only on the flame transfer function for the "compact flame". Predictions using low order methods which account for spatial variation of the thermodynamic properties are seen to better match the reference LEE predictions, and furthermore to improve the match to experimental results, even with the compact flame assumption employed.

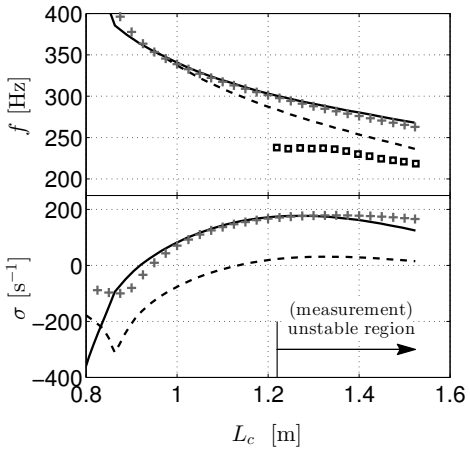

Figure 13: Variation of the first longitudinal modal frequency (top figure) and corresponding growth rate (bottom figure) with the length of the combustion chamber L_c. Markers □: experimental results. Continuous lines: previous prediction using global flame transfer function. Markers +: current prediction using the improved fitted global flame transfer function. Dashed lines: previous prediction using local flame transfer function.

5.3. Low order thermoacoustic model prediction with varying downstream chamber properties

Assuming constant thermodynamic properties within the combustion chamber is likely to be an oversimplification, particularly when the coefficient $\partial\bar{\rho}/\partial x/\bar{\rho}$ in Eq. (40) is large. At the upstream end, reflection of acoustic waves occurs at the interface where the gas temperature and hence the strengths of the acoustic waves change with axial position [57].

Allowing the time-averaged thermodynamic properties to change with axial location complicates the use of analytical solutions. Analytical expressions for the pressure and velocity perturbations associated with special temperature distributions have been derived for cases for which the ratio of specific heats γ is constant[55], but in this work we wish to let this vary.

It was shown in [58] that, when $f > \max(\frac{\bar{c}}{\pi\bar{\rho}}\left|\frac{\partial\bar{\rho}}{\partial x}\right|)$[1], the pressure perturbations can be approximately expressed as:

$$\hat{p}(x) = \left(\frac{\bar{\rho}(x)}{\bar{\rho}(x_f^+)}\right)^{1/4}\left(A_2^+ e^{-i\omega\tau_2(x)} + A_2^- e^{i\omega\tau_2(x)}\right), \qquad x_f^+ \le x \le L_{c,max} \tag{46}$$

where the time delay term $\tau_2(x)$ is expressed as:

$$\tau_2(x) = \int_{x_f^+}^{x} \frac{\mathrm{d}\tilde{x}}{\bar{c}(\tilde{x})} \tag{47}$$

Note that the dependence of the acoustic wave strengths and propagation times on the local thermodynamic properties are both accounted for in these expressions. By substituting Eq. (46) into Eq. (34), the velocity perturbations can be expressed as:

$$\hat{u}(x) = \frac{1}{\bar{\rho}(x)\bar{c}(x)}\left(\frac{\bar{\rho}(x)}{\bar{\rho}(x_f^+)}\right)^{1/4}\left(\left(1-\frac{\beta(x)}{i\omega}\right)A_2^+ e^{-i\omega\tau_2(x)} - \left(1+\frac{\beta(x)}{i\omega}\right)A_2^- e^{i\omega\tau_2(x)}\right), \qquad x_f^+ \le x \le L_{c,max} \tag{48}$$

where

$$\beta(x) = \frac{\bar{c}(x)}{4\bar{\rho}(x)}\frac{\partial\bar{\rho}(x)}{\partial x} \tag{49}$$

[1] In the current configuration, $\min(f) \approx 250$ Hz $> \max(\bar{c}/(\pi\bar{\rho})\,|\partial\bar{\rho}/\partial x|) \approx 50$ Hz.

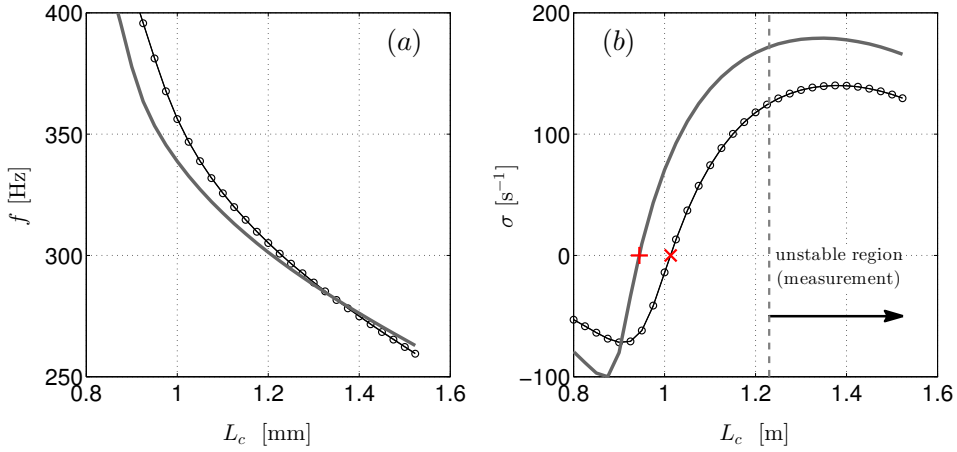

Figure 14: Variation of the first longitudinal modal frequency f (figure (a)) and corresponding growth rates σ (figure (b)) with the length of the combustion chamber L_c. Thin continuous lines: reference predictions from the LEE; thick continuous lines: predictions assuming constant thermodynamic properties; markers ∘: predictions accounting for thermodynamic property variation downstream.

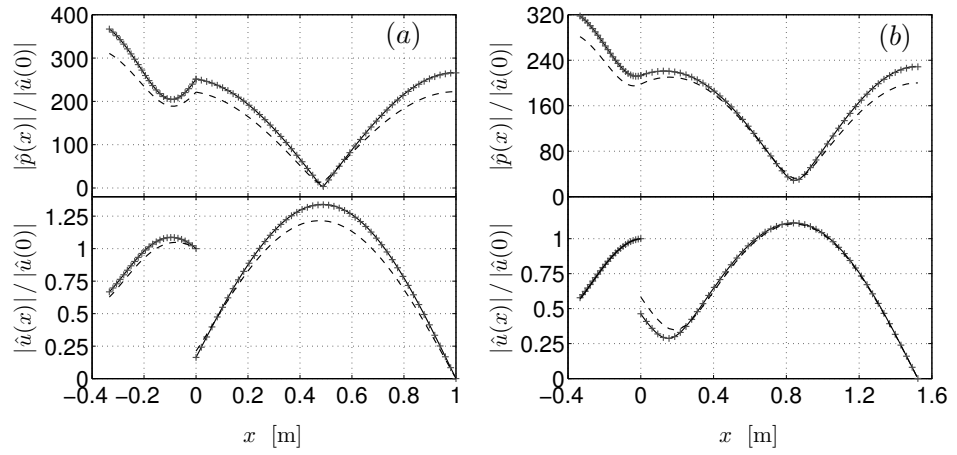

Figure 15: Mode-shapes of the first longitudinal mode. Top figure: normalised pressure perturbations: $|\hat{p}(x)|/|\hat{u}(0)|$, where $\hat{u}(0)$ is the amplitude of velocity perturbation before the flame. Bottom figure: normalised velocity perturbations: $|\hat{u}(x)|/|\hat{u}(0)|$. Continuous lines: reference predictions from the LEE; dashed lines: predictions assuming constant thermodynamic properties; markers +: predictions accounting for thermodynamic property variation downstream. (a): $L_c = 1$ m. (b): $L_c = L_{c,max} = 1.524$ m.

The governing equation (45) is now updated by substituting Eqs. (46) and (48) to give the form:

$$\underbrace{\begin{bmatrix} 1 & -R_1 & 0 & 0 \\ e^{-i\omega L_m/\bar{c}_1} & e^{i\omega L_m/\bar{c}_1} & -1 & -1 \\ \Xi_2(1+\mathcal{DF}(\omega))e^{-i\omega L_m/\bar{c}_1} & -\Xi_2(1+\mathcal{DF}(\omega))e^{i\omega L_m/\bar{c}_1} & \beta(x_f^+)/(i\omega)-1 & \beta(x_f^+)/(i\omega)+1 \\ 0 & 0 & (\beta(L_c)-i\omega)e^{-2i\omega\tau_2(L_c)} & \beta(L_c)+i\omega \end{bmatrix}}_{\mathbf{M_2}} \underbrace{\begin{bmatrix} A_1^+ \\ A_1^- \\ A_2^+ \\ A_2^- \end{bmatrix}}_{\mathcal{A}} = \mathbf{0} \qquad (50)$$

where $\Xi_2 = (S_m/S_c)(\bar{\rho}(x_f^+)\bar{c}(x_f^+))/(\bar{\rho}_1\bar{c}_1)$. The thermoacoustic modes are given by the eigenvalues, ω, which satisfy the dispersion relation $det(M_2) = 0$. The distributions of the thermodynamic properties are accounted for in the time delay term τ_2, while the term $\beta(x)$ affects the acoustic damping and modal growth rate.

The effect of employing this new method, efficiently accounting for the downstream variation of the thermodynamic properties, is shown in Fig. 14. Predictions match perfectly the "reference" values from the LEE, validating the

approximations made in the analytical expression for the acoustic waves.

The modal frequency predicted by assuming constant thermodynamic properties is close to the reference solution at large combustor lengths, the condition from which the values $\overline{T}^*$, $\bar{c}^*$ and $\bar{\rho}^*$ were derived. However, large differences in the growth rate span all combustor lengths. Accounting for the mean thermodynamic property variation in the downstream direction clearly gives an improved match to the reference solution.

The mode-shapes of the pressure and velocity perturbations for the first longitudinal mode are shown in Figure 15 for two combustion chamber lengths L_c = 1 m and $L_c = L_{c,max}$ = 1.524 m. The results accounting for thermodynamic property variation match perfectly the "reference" mode-shape predicted by LEE, with significant dfferences when uniform properties are assumed.

Finally, it is noted that predicted instability onset (denoted by markers + and × in Fig. 14(b)) move closer to the experimentally measured instability onset when the variation of thermodynamic properties is accounted for, even without accounting for the distributed flame transfer function. It would therefore be interesting to combine the ability to account for thermodynamic property variation with a distributed flame transfer function, to see whether good fit to the experimental results can be obtained.

Conclusions

Accurate prediction of thermoacoustic modes depends not only on the geometrical properties of the combustor, but also on accurately calculating the time-averaged thermodynamic properties such as temperature, heat release rate, speed of sound, ratio of specific heats etc., in the different regions of the combustor. Calculation of the global equilibrium properties of fuel combustion is not straightforward due to complex multi-species and multi-step reaction mechanisms. Even calculations accounting for few species (e.g., 6 major species CO_2, CO, H_2O, H_2, O_2 and N_2 for hydrocarbon-air combustion are used in this work) are still not straightforward since multiple partial equilibrium equations with multiple unknowns need to be simultaneously determined, becoming yet more complicated when the flame temperature is to be determined. A method decoupling the calculations of species dissociations has been proposed in this work to reduce the calculation cost and improve the precision when using few species. This method is extended to the calculation of mole fractions, temperature, heat release rate, speed of sound and ratio of specific heats of the combustion products of hydrocarbon-air flames. Validation was carried out by changing the equivalence ratio, initial temperature, ambient pressure and fuel. Results were compared to those computed using the CANTERA code with the GRI-Mech 3.0 mechanism, comprising 325 elementary chemical reactions with associated rate coefficient expressions and thermochemical parameters for the 53 species. The match was perfect, even for high initial temperatures and large ambient pressures. The proposed method is thus a reliable and efficient method, which can be easily embedded in low-order thermoacoustic prediction tools.

Due to their ability to capture the key physics combined with computational efficiency, low-order wave-based network models have been widely used in the analysis of thermoacoustic instabilities. Typically, the combustion chamber is considered as an acoustic element with uniform thermodynamic properties, greatly simplifying the calculation of the mode frequencies and growth rates. However, this approach has been shown to lack sufficient quantitative accuracy when large temperature changes occur along the combustion chamber. Approximations of acoustic waves in a uniform duct with a smoothly-varying temperature distribution were incorporated into a thermoacoustic network model. This was found to improve thermoacoustic modal predictions of the combustor. Future work will seek to combine varying thermodynamic properties with distributed flame transfer functions in order to further improve predictive capability.

Acknowledgement

The authors would like to gratefully acknowledge the European Research Council (ERC) Starting Grant (grant no.305410) ACOULOMODE (2013-2018) for supporting the current research.

References

[1] S. M. Correa, Power generation and aeropropulsion gas turbines: From combustion science to combustion technology, *P. Combust. Inst.* 27 (1998) 1793–1807.

[2] S. Candel, Combustion dynamics and control: Progress and challenges, *P. Combust. Inst.* 29 (2002) 1–28.

[3] T. Lieuwen, V. Yang (Eds.), *Combustion instabilities in gas turbines, Operational experience, Fundamental mechanisms, and Modeling*, vol. 210 of *Progress in Astronautics and Aeronautics*, AIAA, Inc., Reston, Virginia, 2005.
[4] M. S. Howe, *Acoustic of fluid-structure interactions*, Cambridge University Press, London, 1998.
[5] H. Levine, J. Schwinger, On the radiation of sound from an unflanged circular pipe, *Phys. Rev.* 73 (1948) 383–406.
[6] T. Lieuwen, B. T. Zinn, The role of equivalence ratio oscillations in driving combustion instabilities in low NOx gas turbines, *P. Combust. Inst.* 27 (1998) 1809–1816.
[7] H. M. Altay, R. L. Speth, D. E. Hudgins, A. F. Ghoniem, The impact of equivalence ratio oscillations on combustion dynamics in a backward-facing step combustor, *Combust. Flame* 156 (2009) 2106–2116.
[8] G. H. Markstein, W. Squire, On the Stability of a Plane Flame Front in Oscillating Flow, *J. Acoust. Soc. Am.* 27 (1955) 416–424.
[9] G. Searby, D. Rochwerger, A parametric acoustic instability in premixed flames, *J. Fluid Mech.* 231 (1991) 529–543.
[10] X. Wu, C. K. Law, Flame-acoustic resonance initiated by vortical disturbances, *J. Fluid Mech.* 634 (2009) 321–357.
[11] R. C. Assier, X. Wu, Linear and weakly nonlinear instability of a premixed curved flame under the influence of its spontaneous acoustic field, *J. Fluid Mech.* 758 (2014) 180–220.
[12] L. Gicquel, G. Staffelbach, T. Poinsot, Large Eddy Simulations of gaseous flames in gas turbine combustion chambers, *Prog. Energ. Combust.* 38 (2012) 782–817.
[13] L. Selle, G. Lartigue, T. Poinsot, R. Koch, K.-U. Schildmacher, W. Krebs, B. Prade, P. Kaufmann, D. Veynante, Compressible large eddy simulation of turbulent combustion in complex geometry on unstructured meshes, *Combust. Flame* 137 (2004) 489–505.
[14] G. Staffelbach, L. Gicquel, G. Boudier, T. Poinsot, Large Eddy Simulation of self excited azimuthal modes in annular combustors, *P. Combust. Inst.* 32 (2009) 2909–2916.
[15] L. Crocco, Aspects of Combustion Stability in Liquid Propellant Rocket Motors Part I: Fundamentals. Low Frequency Instability With Monopropellants, *J. Am. Rocket. Soc.* 21 (1951) 163–178.
[16] A. P. Dowling, Nonlinear self-excited oscillations of a ducted flame, *J. Fluid Mech.* 346 (1997) 271–290.
[17] R. Balachandran, B. O. Ayoola, C. Kaminski, A. P. Dowling, E. Mastorakos, Experimental investigation of the nonlinear response of turbulent premixed flames to imposed inlet velocity oscillations, *Combust. Flame* 143 (2005) 37–55.
[18] D. Durox, T. Schuller, N. Noiray, S. Candel, Experimental analysis of nonlinear flame transfer functions for different flame geometries, *P. Combust. Inst.* 32 (2009) 1391–1398.
[19] T. Schuller, D. Durox, S. Candel, A unified model for the prediction of laminar flame transfer functions: comparisons between conical and V-flame dynamics, *Combust. Flame* 134 (2003) 21–34.
[20] J. Li, A. S. Morgans, Time domain simulations of nonlinear thermoacoustic behaviour in a simple combustor using a wave-based approach, *J. Sound Vib.* 346 (2015) 345–360.
[21] X. Han, A. S. Morgans, Simulation of the flame describing function of a turbulent premixed flame using an open-source {LES} solver, *Combust. Flame* 162 (2015) 1778–1792.
[22] X. Han, J. Li, A. S. Morgans, Prediction of combustion instability limit cycle oscillations by combining flame describing function simulations with a thermoacoustic network model, *Combust. Flame* 162 (2015) 3632–3647.
[23] T. C. Lieuwen, Experimental Investigation of Limit-Cycle Oscillations in an Unstable Gas Turbine Combustor , *J. Propul. Power* 18 (2002) 61–67.
[24] T. Poinsot, D. Veynante, *Theoretical and Numerical Combustion*, R.T. Edwards Inc, Philadelphia, Pennsylvania, 2005.
[25] C. F. Silva, F. Nicoud, T. Schuller, D. Durox, S. Candel, Combining a Helmholtz solver with the flame describing function to assess combustion instability in a premixed swirled combustor, *Combust. Flame* 160 (2013) 1743–1754.
[26] X. Wu, M. Wang, P. Moin, N. Peters, Combustion instability due to the nonlinear interaction between sound and flame, *J. Fluid Mech.* 497 (2003) 23–53.
[27] X. Wu, P. Moin, Large-activation-energy theory for premixed combustion under the influence of enthalpy fluctuations, *J. Fluid Mech.* 655 (2010) 3–37.
[28] S. S. Stow, LOTAN: Low-Order Thermo-Acoustic Network model, Tech. Rep., Cambridge University, Cambridge, 2005.
[29] N. Noiray, D. Durox, T. Schuller, S. Candel, A unified framework for nonlinear combustion instability analysis based on the flame describing function., *J. Fluid Mech.* 615 (2008) 139–167.
[30] P. Palies, D. Durox, T. Schuller, S. Candel, Nonlinear combustion instability analysis based on the flame describing function applied to turbulent premixed swirling flames, *Combust. Flame* 158 (2011) 1980–1991.
[31] K. Kim, J. Lee, B. Quay, D. Santavicca, Spatially distributed flame transfer functions for predicting combustion dynamics in lean premixed gas turbine combustors, *Combust. Flame* 157 (2010) 1718–1730.
[32] P. Schmitt, T. Poinsot, B. Schuermans, K. P. Geigle, Large-eddy simulation and experimental study of heat transfer, nitric oxide emissions and combustion instability in a swirled turbulent high-pressure burner, *J. Fluid Mech.* 570 (2007) 17–46.
[33] B. Franzelli, E. Riber, M. Sanjosé, T. Poinsot, A two-step chemical scheme for kerosene-air premixed flames, *Combust. Flame* 157 (2010) 1364–1373.
[34] D. G. Goodwin, H. K. Moffat, R. L. Speth, Cantera: An Object-oriented Software Toolkit for Chemical Kinetics, Thermodynamics, and Transport Processes, `http://www.cantera.org`, version 2.1.2, 2014.
[35] G. Stiesch, *Modeling Engine Spray and Combustion Processes*, Springer, Berlin, 2003.
[36] K. K.-y. Kuo, *Principles of Combustion*, John Wiley and Sons Inc., New Jersey, 2005.
[37] S. R. Turns, *An Introduction to Combustion: Concepts and Applications, third edition*, McGraw-Hill, New York, 2012.
[38] C. K. Law, *Combustion Physics* , Cambridge university press, Cambridge, 2006.
[39] A. H. Lefebvre, D. R. Ballal, *Gas Turbine Combustion: Alternative Fuels and Emissions, Third Edition*, CRC Press, Boca Raton, Florida, 2010.
[40] C. Law, A. Makino, T. Lu, On the off-stoichiometric peaking of adiabatic flame temperature, *Combust. Flame* 145 (2006) 808–819.
[41] P. Clavin, F. A. Williams, Effects of molecular diffusion and of thermal expansion on the structure and dynamics of premixed flames in turbulent flows of large scale and low intensity, *J. Fluid Mech.* 116 (1982) 251–282.

[42] M. Matalon, B. J. Matkowsky, Flames as gasdynamic discontinuities, *J. Fluid Mech.* 124 (1982) 239–259.
[43] A. P. Dowling, The calculation of thermoacoustic oscillations, *J. Sound Vib.* 180 (1995) 557–581.
[44] R. J. Kee, J. F. Grcar, M. D. Smooke, J. A. Miller, E. Meeks, *PREMIX: A FORTRAN Program for Modeling Steady Laminar One-Dimensional Premixed Flames*, URL `http://www.ewp.rpi.edu/hartford/~ernesto/F2014/MMEES/Papers/ENERGY/4NaturalGas/PREMIX-1998-Sandia.pdf`, 1998.
[45] J. Li, F. Richecoeur, T. Schuller, Determination of heat release rate disturbances in open flames based on fluctuations in the travel time of ultrasonic waves, *Combust. Sci. Technol.* 184 (2012) 533–555.
[46] J. Li, F. Richecoeur, T. Schuller, Reconstruction of heat release rate disturbances based on transmission of ultrasounds: Experiments and modeling for perturbed flames, *Combust. Flame* 160 (2013) 1779–1788.
[47] J. Li, D. Durox, F. Richecoeur, T. Schuller, Analysis of chemiluminescence, density and heat release rate fluctuations in acoustically perturbed laminar premixed flames, *Combust. Flame* 162 (2015) 3934–3945.
[48] C. S. Goh, A. S. Morgans, The Influence of Entropy Waves on the Thermoacoustic Stability of a Model Combustor, *Combust. Sci. Technol.* 185 (2013) 249–268.
[49] H. Meng, V. Yang, A unified treatment of general fluid thermodynamics and its application to a preconditioning scheme, *J. Comput. Phys.* 189 (2003) 277–304.
[50] A. P. Dowling, S. R. Stow, Acoustic Analysis of Gas Turbine Combustors, *J. Propul. Power* 19 (2003) 751–764.
[51] B. Schuermans, *Modeling and control of thermoacoustic instabilities*, Ph.D. thesis, École Polytechnique Fédérale de Lausanne, Lausanne,Switzerland, 2003.
[52] J. Li, D. Yang, C. Luzzato, A. S. Morgans, OSCILOS: the open source combustion instability low order simulator, Tech. Rep., Imperial College London, http://www.oscilos.com, 2014.
[53] B. D. Bellows, Y. Neumeier, T. Lieuwen, Forced Response of a Swirling, Premixed Flame to Flow Disturbances, *J. Propul. Power* 22 (2006) 1075–1084.
[54] K. Kim, J. Lee, H. Lee, B. Quay, D. Santavicca, Characterization of Forced Flame Response of Swirl-Stabilized Turbulent Lean-Premixed Flames in a Gas Turbine Combustor, *J. Eng. Gas Turbines Power* 132 (2010) 041502(8 pages).
[55] R. Sujith, G. Waldherr, B. Zinn, An exact solution for one-dimensional acoustic fields in ducts with an axial temperature gradient, *J. Sound Vib.* 184 (1995) 389–402.
[56] K. Wieczorek, *Numerical study of Mach number effects on combustion instability*, Ph.D. thesis, Université Montpellier II, 2010.
[57] T. Lieuwen, *Unsteady Combustor Physics*, Cambridge University Press, Cambridge, 2012.
[58] A. Cummings, Ducts with axial temperature gradients: An approximate solution for sound transmission and generation, *J. Sound Vib.* 51 (1977) 55–67.